# Transport Modeling for W7-X on the Basis of W7-AS Experimental Results

C.D. Beidler, J. Geiger, H. Maaßberg, N.B. Marushchenko, Yu. Turkin, W7-AS Team

*Max-Planck Institut für Plasmaphysik*
*IPP-EURATOM Association, Greifswald Germany*

October 12, 2007

Exploratory simulations of plasma confinement in the Wendelstein 7-X (W7-X) stellarator are presented, concentrating on scenarios which simultaneously achieve high temperature and high $\beta$ (normalized plasma pressure) at the full magnetic field of $B = 2.5$ T. Efficient 1-D transport and ray-tracing codes are combined to provide an approximately self-consistent description of the heating and current drive (ECCD) to be expected from up to 10 MW of electron cyclotron resonance heating (ECRH) in W7-X. Best performance is exhibited in high density ($n = 1.8 \times 10^{20}$ m$^{-3}$) simulations heated at the second harmonic of the ordinary mode, although control of the magnetic topology at the plasma edge — needed to insure functioning of the island divertor — becomes problematic due to the imbalance of the bootstrap current and ECCD.

Keywords: Wendelstein 7-X, neoclassical transport, bootstrap current, electron cyclotron current drive.

The design specifications of the Wendelstein 7-X (W7-X) stellarator were chosen so as to enable this device to demonstrate the reactor potential of the advanced stellarator concept. The ultimate goal of the experimental program is thus to heat, confine and exhaust plasmas with reactor-relevant $\beta$ and collisionality values under steady-state conditions. This goal must be viewed in its entirety, and it is therefore mandatory to avoid the common experimental expedient of breaking it up into a number of self-exclusive portions (e.g. performing "high-$\beta$" experiments at small values of the magnetic field or "low-collisionality" experiments by reducing the density). Currently, there exists no single numerical tool capable of simulating all aspects of such a multifaceted problem but exploratory investigations have been carried out to determine the expected range of W7-X plasma parameters assuming electron cyclotron resonance heating (ECRH) and the prospects for magnetic configuration control using the accompanying current drive (ECCD). The results of these investigations are the subject of this paper.

The basis for these investigations is provided by the theoretical interpretation of experimental results from the W7-AS device, which operated in Garching, Germany, from 1988 until 2002. Three observations are of principal importance for the simulations carried out here:

(1) With the exception of the low-temperature edge region, high-performance W7-AS discharges (with central densities $n(0) > 5 \times 10^{19}$ m$^{-3}$ and central ion and electron temperatures $T^{i,e}(0) > 1$ keV) were described well by the predictions of stellarator neoclassical theory. This was true for all quantities of interest including the radial particle fluxes, energy fluxes and ambipolar electric field

[1] as well as the bootstrap current [2, 3]. For the radial losses, this may be attributed to the strong temperature dependence of the neoclassical transport coefficients in the so-called $1/\nu$ regime, which scale

$$\propto \frac{\epsilon_{eff}^{3/2} T^{7/2}}{n B_0^2 R_0^2}$$

where $\epsilon_{eff}$ is the effective helical ripple (a measure of how well a stellarator's magnetic field confines trapped particles), $B_0$ is the magnitude of the magnetic field and $R_0$ is the major radius of the torus. For W7-AS, a device with moderate values of $\epsilon_{eff}$, this led to neoclassical energy diffusivities $\chi > 1$ m$^2$/s when $T > 1.5$ keV at $n = 10^{20}$ m$^{-3}$. Although W7-X was optimized to have much smaller values of $\epsilon_{eff}$, the temperature dependence of this scaling remains unchanged and justifies the continued relevance of neoclassical theory for describing high-temperature bulk plasmas in W7-X.

(2) The low-temperature periphery of W7-AS discharges exhibited anomalously large radial transport, considerably in excess of neoclassical expectations. Assuming this anomalous transport to be purely diffusive, a data set of experimental profiles for ECRH discharges was used to solve the local energy balance in the gradient region and to determine the dependence of the energy diffusivity on local plasma parameters using linear regression; results found that $\chi$ was inversely proportional to density and independent of temperature [4]. This result is noteworthy as the density scaling is identical to that of $1/\nu$ transport so that a simple "combination" of these anomalous and neoclassical results would predict a global energy confinement time obeying $\tau_E \propto n$ (assuming $n$ is varied while holding its profile shape constant). Experimental results for such a density scan are shown in Fig. 1 for two different W7-AS
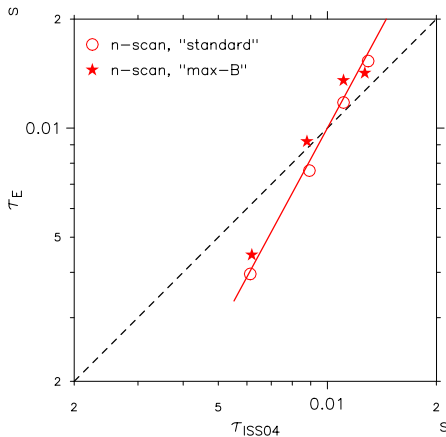
Fig. 1 Energy confinement times for 1.2 MW ECRH discharges in two W7-AS configurations for different central densities compared to the expectations of ISS04. A linear scaling of $\tau_E$ with $n$ is shown by the red line.

magnetic configurations heated by 1.2 MW ECRH. A linear scaling of $\tau_E$ with density is indicated by the red line and describes the results considerably better than the $n^{0.54}$ dependence of the International Stellarator Scaling ISS04 [5] which is shown by the dashed line for comparison.

(3) A linear description of ECCD using the adjoint approach with a Spitzer function modified to account for trapped-particle effects provided an excellent description of electron cyclotron current drive experiments in W7-AS at densities of $6 \times 10^{19}$ m$^{-3}$ and larger [3]. As a consequence, high-density ECRH simulations in W7-X can accurately model both power deposition and ECCD using the ray-tracing technique without the need to resort to lengthy solutions of the Fokker-Planck equation.

At the moment, simulations are restricted to a handful of fixed W7-X equilibria which are calculated using VMEC [6] for specified pressure profiles. Modifications of the equilibrium caused by internal current densities (due to ECCD and the bootstrap current) or changes in the pressure profile are not accounted for. For each equilibrium the mono-energetic neoclassical transport coefficients are determined using the Drift Kinetic Equation Solver (DKES) [7] for the relevant range of electric field, $E_r$, and collisionality values on several magnetic flux surfaces (typically entailing more than 3000 individual DKES calculations); routines are also provided for interpolation of intermediate values in this three-dimensional space and to perform the energy convolutions necessary to calculate the neoclassical transport matrix. With the specification of a model for the anomalous energy diffusivity (based on W7-AS results, $\chi_{an} = 10^{19} n^{-1}$ m$^2$/s is taken here) one has sufficient information to solve a system of four coupled diffusion equations for the radial profiles of $T^e$, $T^i$, $E_r$ and the toroidal plasma current using a 1-D transport code [8]; the density profile is held fixed for these simulations so that a model for the anomalous particle diffusion coefficient is not re-

quired. Heating of the plasma by ECRH and calculations of the associated ECCD are simulated with the ray-tracing code TRAVIS [9]. Through direct coupling with the transport code, temperature effects on the ECRH deposition and the current-drive efficiency are fully accounted for. Radiation losses have been ignored for these simulations and impurities are only accounted for insofar as an effective charge number $Z_{eff} = 1.5$ is assumed to exist throughout the plasma.

The ECRH system of W7-X will consist of ten 1 MW gyrotrons, designed for thirty minutes of continuous wave operation at a frequency of 140 GHz (resonant at $B = 2.5$ T) [10]. Operation at the second harmonic of the extraordinary mode (X2) offers an extremely flexible means of heating the plasma due to its excellent first-pass absorption, allowing a wide choice of launch angles and thus the ability to vary the ECCD over a broad range of values in both the co- and counter-directions (by convention, current in the co-direction increases the rotational transform, $\iota$, and decreases it when flowing in the counterdirection). A limitation is the X2 density cut-off which occurs at $n^e = 1.2 \times 10^{20}$ m$^{-3}$, roughly a factor of two less than possible if operation is switched to the second harmonic of the ordinary mode (O2). Unfortunately, firstpass absorption of O2 ECRH is relatively poor for the projected plasma temperatures in W7-X, forcing the adoption of a multi-pass absorption scheme with a fixed launching geometry to conform to the placement of mirrors and reflecting surfaces within the vacuum vessel. This launching geometry has been chosen to provide equal ECCD in the co- and counter-directions so that full-power operation implies doing without any net driven current. This drawback is not as serious as it might seem, however, since the current-drive efficiency falls rapidly with increasing density, regardless.

High-density O2 operation in W7-X is potentially of critical importance for optimum divertor performance in the device. Preliminary simulations with the 3-D edge package EMC3/EIRENE [11] have shown that pumping of neutral gas in the W7-X divertor geometry becomes efficient at edge densities of at least $3 \times 10^{19}$ m$^{-3}$ [12]; a similar value of the edge density was found to provide the impurity screening effect observed experimentally in W7-AS HDHdischarges. Ratios of central to edge density in W7-AS were seldom less than five making it appear questionable whether such high edge densities can be reached in W7-X with X2 ECRH. Heating with O2 was not attempted in W7-AS but is the most attractive option for high-density operation in the early W7-X campaigns as neutral-beaminjection heating will be limited to ten-second pulses during this time.

The requirement of sufficient ECCD to balance the bootstrap current is also a consequence of the divertor concept chosen for W7-X. This makes use of the naturally occurring magnetic islands with $\iota = 5/m$ at the plasma edge (configurations with $m = 4$, 5 or 6 may be realized with
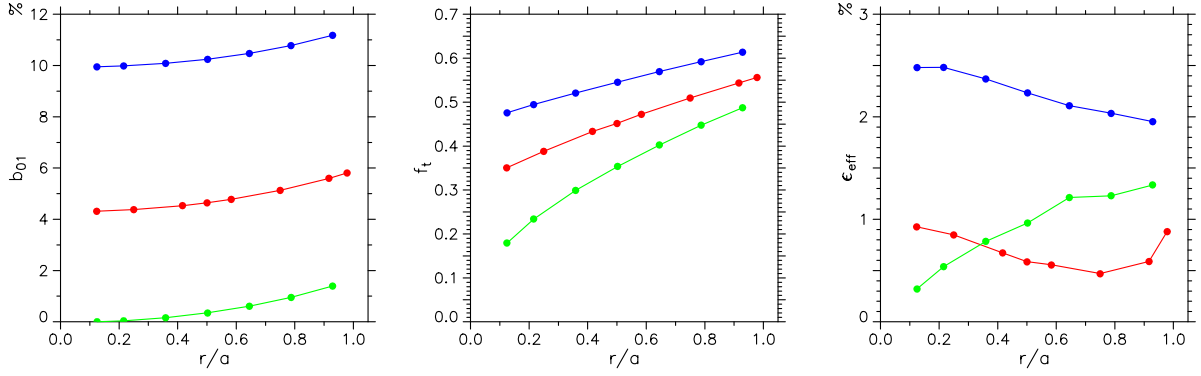
Fig. 2 Radial profiles of the toroidal mirror harmonic (left), the fraction of trapped particles (center) and the effective helical ripple (right) for the W7-X high-mirror (blue), standard (red) and low-mirror (green) configurations.

the W7-X coil system) to guide the outflowing plasma into prepared divertor regions where recycling and exhaust is to take place. For this "island divertor" concept to be effective the magnetic topology of the edge region must be maintained throughout the discharge, which is equivalent to preserving the original value of the rotational transform at the edge. This is possible to sufficient accuracy for net plasma currents of the order ±10 kA.

## Simulation Results

The simulations presented here were performed for three different W7-X configurations with the currents in the modular coils chosen to either increase or decrease the magnitude of the toroidal mirror term in $B$ relative to a standard case. (Having the designation $b_{01}$ in the poloidal-, toroidal-angle Fourier decomposition of $B$, the toroidal mirror is also commonly referred to as the "bumpiness" of the magnetic field strength.) Radial profiles of relevant quantities for the vacuum fields are plotted in Fig. 2. The high-mirror configuration (blue curves) has the largest fraction of trapped particles ($f_t$) at all radii which generally helps to reduce the bootstrap current while the low-mirror configuration (green curves) provides the opposite extreme. With regard to confinement, however, the standard configuration (red curves) has the smallest values of $\epsilon_{eff}$ over most of the plasma radius and these values are further reduced by finite-$\beta$ effects, especially near the plasma axis. With its much larger $\epsilon_{eff}$, the high-mirror configuration can be expected to have the poorest confinement of these three. The fraction of trapped particles is also of relevance to the current-drive efficiency with small values of $f_t$ most conducive for maximizing ECCD. It will be noted that the simultaneous goals of minimum bootstrap current, maximum confinement and maximum ECCD are contradictory and that the simulations are therefore also a means to search for the best compromise.

A first set of simulations was carried out to determine whether compensation of the bootstrap current by ECCD is possible in all W7-X configurations assuming X2 heating at a density value close to cut-off. The bootstrap current flows in the co-direction in these simulations so that the launch angles of the ECRH system were chosen to maximize counter-ECCD. For significant counter-current near the axis the rotational transform goes to zero in the vicinity, implying a loss of confinement in this region. Indeed, for similar discharges in W7-AS, this loss of confinement was clearly indicated by flat temperature profiles throughout the $\iota \approx 0$ portion of the plasma [3]. Such an effect is not accounted for in the present simulations as self-consistent alterations to the equilibrium are not attempted (the original equilibrium with $\iota(0) > 5/6$ is maintained during the simulation). To avoid this difficulty, off-axis heating was also considered; an example of the results for the $<\beta> = 2\%$ equilibrium of the W7-X standard configuration with 10 MW ECRH is presented in Fig. 3. The shift of the ECCD current density away from the plasma axis (green curve labeled $J_{cd}$ in the lower center) conforms closely to the deposition profile (lower left). The total driven current in this simulation, $I_{ECCD} = -88$ kA, is more than sufficient to compensate the bootstrap current of $I_{bs} = 75$ kA as evinced by the slight reduction of the edge rotational transform relative to the current-free VMEC equilibrium value (compare black and green $\iota$ curves on the lower right). The significant reduction of the rotational transform over a large portion of the plasma is the price one pays for using ECCD to compensate the bootstrap current (due to the inherent mismatch of the current-density profiles); nevertheless, $\iota$ remains well above zero for off-axis deposition. The simulation results yield $<\beta> = 2.70\%$, in reasonably good agreement with the assumed equilibrium.

The impact which the magnetic configuration has on the results can be illustrated by considering a similar off-axis X2 simulation for the high-mirror W7-X. As shown in Fig. 4, the bootstrap current density assumes small values over the entire plasma radius due to the approximate cancellation of the ion and electron contributions. The negative $J_{bs}^e$ is due to the lower temperatures reached in this
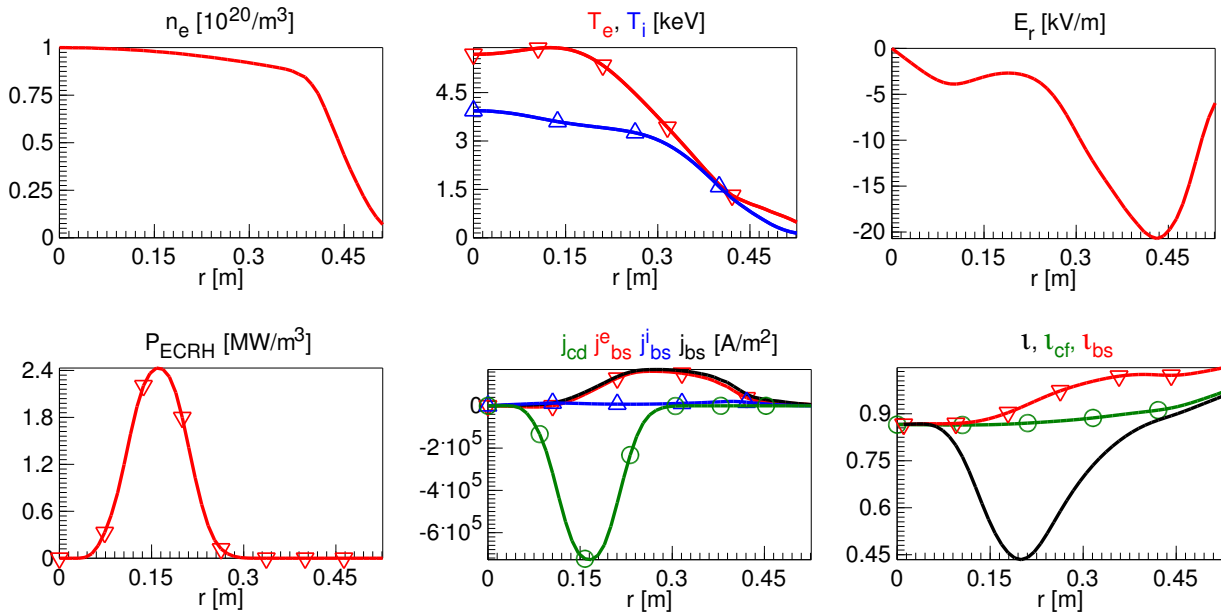
**Fig. 3** Simulation results for 10 MW off-axis X2 ECRH in the $<\beta> = 2\%$ standard configuration. Density, temperature and radial electric field profiles are plotted in the upper row; power deposition, current densities and rotational transform are given in the lower row. In the temperature plot, $T^e$ is shown in red, $T^i$ in blue. In the current density plot, $J_{cd}$ is given in green, $J^e_{bs}$ in red, $J^i_{bs}$ in blue and the total bootstrap current density in black. In the rotational transform plot, the current-free (VMEC equilibrium) $\iota$ is shown in green, the alteration of this profile due to the bootstrap current appear in red and the rotational transform profile accounting for all currents is given in black.
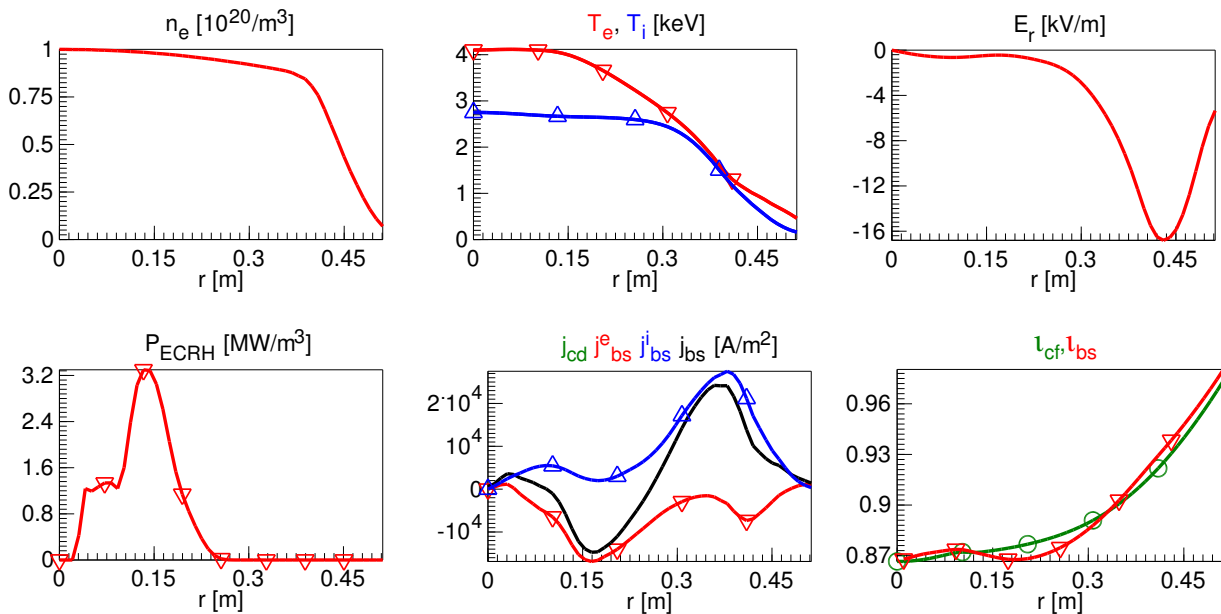
**Fig. 4** As in Fig. 3 for 10 MW off-axis X2 ECRH in the vacuum high-mirror configuration.

simulation, shifting the collisionality to higher values where the helical components of the magnetic field are predominant and can reverse the sign of the bootstrap current coefficients. $I_{ECCD}$ as large as $-48$ kA can be achieved in the high-mirror configuration but is not required for this simulation as the residual bootstrap current is only $I_{bs} = 6$ kA, which has little effect on the rotational transform profile (red curve on the lower right). The poorer confinement also reduces the normalized plasma pressure to $<\beta>= 2.40\%$.

A summary of the X2 results is provided in Fig. 5 which depicts the values of $I_{bs}$, $I_{ECCD}$ and the plasma stored energy, $W$, for on-axis and off-axis heating simulations as a function of the axis value of $b_{01}$ for the equilibrium. From largest to smallest value of $b_{01}$, these equilibria are for the high-mirror vacuum, standard vacuum, standard $<\beta>= 2\%$, standard $<\beta>= 4\%$ and low-mirror vacuum configurations. The toroidal mirror is reduced by increasing plasma pressure; as already noted, this is expected to improve confinement in the standard configuration which is indeed verified by the increase in $W$. At the same time, however, both $I_{bs}$ and $I_{ECCD}$ are significantly increased. Also as expected, confinement is poorest in the high-mirror configuration. The stored energy is nearly independent of the deposition profile so that off-axis heating must be favored due to its more benign effects on the rotational transform profile.

For O2 operation current drive can only be realized by doing without a portion of the ECRH power. To maximize the counter-ECCD, the five gyrotrons which would provide co-ECCD are therefore not utilized, limiting the heating power to 5 MW. Additionally, O2 absorption is a strong function of the electron temperature so that O2 ECRH is only possible when a high-$T^e$ "target" plasma is already in existence before O2 heating is begun. This is the basis for the series of simulations which are summarized in Fig. 6, which were performed in the $<\beta>= 2\%$ standard configuration. Here X2 heating is assumed at low to moderate densities but with the identical launching geometry necessary for O2 operation; as in the previous X2 simulations, $I_{ECCD}$ exceeds $I_{bs}$ at all densities with their sum $\approx -12$ kA at $n = 10^{20}$ m$^{-3}$ (note that $-I_{ECCD}$ has been plotted in the figure). For O2 operation at this density, however, the ECCD is considerably reduced with its magnitude falling below that of the bootstrap current which is only slightly affected through the differing ECRH deposition profiles of X2 and O2. At higher densities, the "gap" between the two currents closes but is probably initially too great to expect an adequate degree of configuration control during a simple density ramp.

For scenarios where ECCD compensation of the bootstrap current is not possible, there remains the option of factoring the resulting change in the edge value of the rotational transform into the experimental plans. For example, a vacuum magnetic configuration could be chosen with an
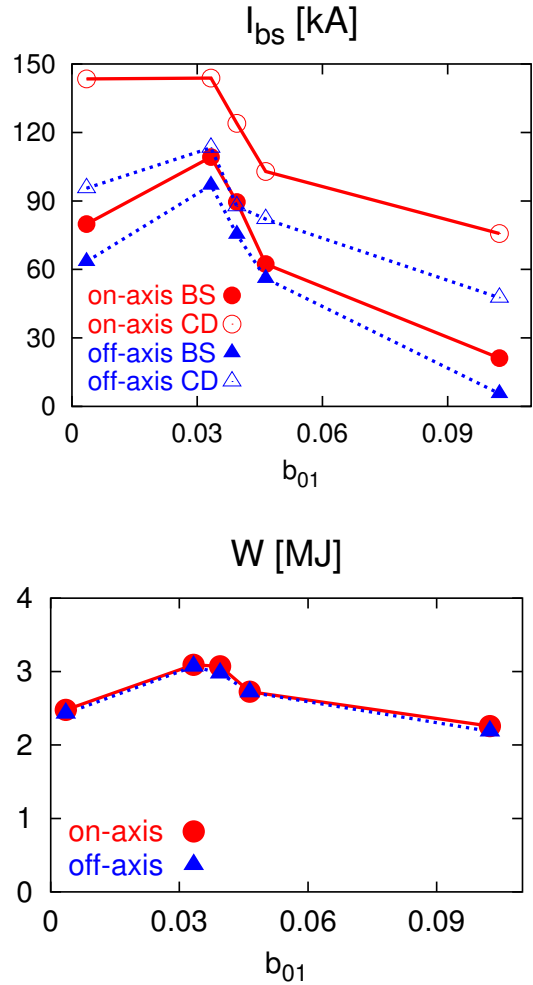


Fig. 5 Values of the bootstrap current and ECRH driven current (top) and plasma stored energy (bottom) as functions of the axis value of the toroidal mirror for X2 simulations with on-axis and off-axis deposition.
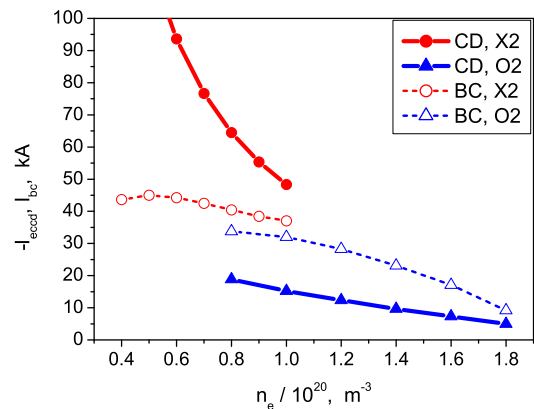


Fig. 6 Values of the bootstrap current and ECRH driven current for 5 MW ECRH simulations in the $<\beta>= 2\%$ standard configuration. The X2 simulations were performed with the O2 launching geometry.

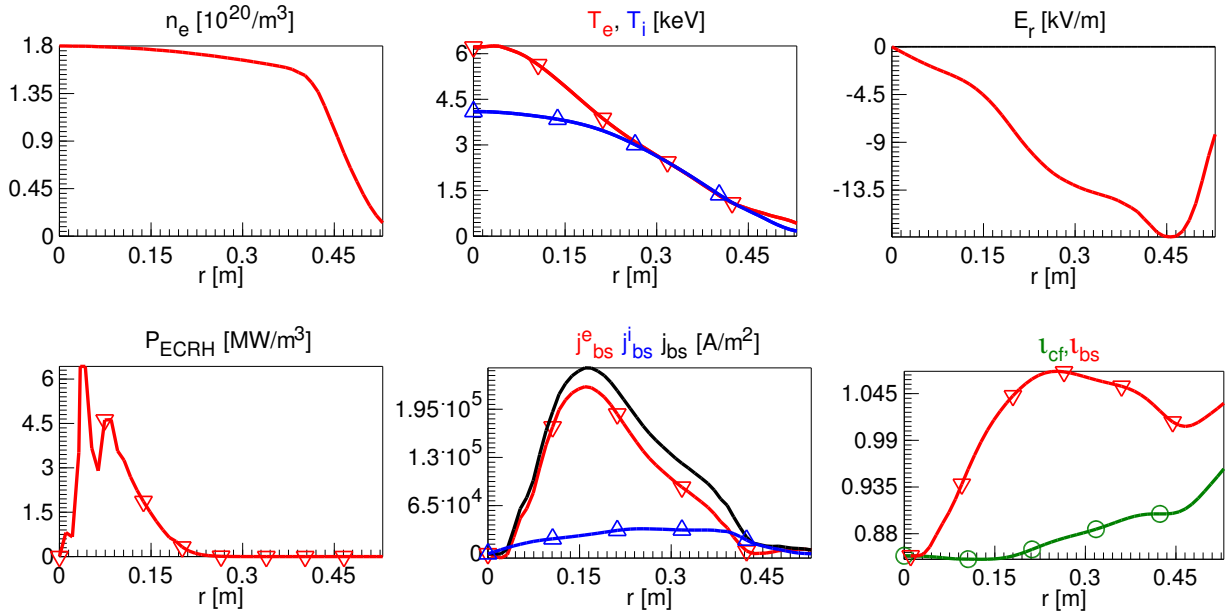Fig. 7   As in Figure 3 for 10 MW on-axis O2 ECRH in the $<\beta>= 4\%$ standard configuration.

edge $\iota$ reduced by an amount which is then to be provided by the net current of the planned discharge. Such a scenario poses additional complications since one must provide co-ECCD at the initial stage to provide the "missing" bootstrap current and be able to adjust the ECCD during later stages according to the changes in $I_{bs}$. This is plausible using X2 heating and offers the only opportunity for subsequently continuing with the discharge, transferring the full 10 MW of ECRH into the O2 mode. At the moment, such simulations are beyond the capabilities of the approach used here, but it is possible to determine the magnitude of the bootstrap current in the steady-state portion of such a discharge. Results for 10 MW on-axis O2 ECRH assuming a central density of $1.8 \times 10^{20}$ m$^{-3}$ are given in Fig. 7 for the $<\beta>= 4\%$ standard configuration. The total bootstrap current of 82 kA determined for this simulation and its rather peaked current density profile lead to the alteration of the $\iota$ profile shown in red on the lower right. It is expected that a more monotonic profile of $\iota$ can be realized by shifting the deposition off axis, although this is likely to result in a modest deterioration of the 97.5% three-pass absorption for the O2 heating in this simulation and in the $<\beta>= 4.13\%$ value which on-axis deposition makes possible.

From the preceding discussion it is clear that time-dependent discharge scenarios will be high on the priority list of future tasks. Near-term plans also include determining free-boundary VMEC equilibria with the pressure profiles and internal current densities calculated here so as to enable modeling of the magnetic field topology in the (assumed) vacuum region outside the last-closed-flux-surface. This will enable one to reach a considerably more detailed verdict concerning the compatibility of edge topology with the island divertor than was possible in the present work

where only the edge value of $\iota$ was considered.

[1] J. Baldzuhn, M. Kick, H. Maaßberg and the W7-AS Team, Plasma Phys. Control. Fusion **40**, 967 (1998).
[2] V. Erckmann, U. Gasparino and H. Maaßberg, Plasma Phys. Control. Fusion **34**, 1917 (1992).
[3] H. Maaßberg *et al.*, Plasma Phys. Control. Fusion **47**, 1137 (2005).
[4] H. Ringler *et al.*, Plasma Phys. Control. Fusion **32**, 933 (1990).
[5] H. Yamada *et al.*, Nucl. Fusion **45**, 1684 (2005).
[6] S.P. Hirshman, W.I. van Rij and P. Merkel, Comput. Phys. Comm. **43**, 143 (1986).
[7] W.I. van Rij and S.P. Hirshman, Phys. Fluids B **1**, 563 (1989).
[8] Yu. Turkin, H. Maaßberg, C.D. Beidler, J. Geiger and N.B. Marushchenko, Fusion Sci. Technol. **50**, 387 (2006).
[9] N.B. Marushchenko *et al.*, Plasma Fusion Res. **2**, S1000 (2007).
[10] V. Erckmann *et al.*, Fusion Sci. Technol. **52**, 291 (2007).
[11] Y. Feng *et al.*, Contrib. Plasma Phys. **44**, 57 (2004).
[12] D. Sharma, Y. Feng, F. Sardei and D. Reiter, Nucl. Fusion **45**, 825 (2005).